Normalization of Intrinsic Neural Circuits Governing Tourette's Syndrome Using Cranial Electrotherapy Stimulation

Jianping Qiao, Shenhong Weng, Pengwei Wang, *Member, IEEE*, Jun Long, and Zhishun Wang*, *Senior Member, IEEE*

Abstract*—*Goal: **The aim of this study was to investigate the normalization of the intrinsic functional activity and connectivity of TS adolescents before and after the cranial electrotherapy stimulation (CES) with alpha stim device.** ***Methods:*** **We performed resting-state functional magnetic resonance imaging on eight adolescents before and after CES with mean age of about nine-years old who had Tourette's syndrome with moderate to severe tics symptom. Independent component analysis (ICA) with hierarchical partner matching method was used to examine the functional connectivity between regions within cortico-striato-thalamo-cortical (CSTC) circuit. Granger causality was used to investigate effective connectivity among these regions detected by ICA. We then performed pattern classification on independent components with significant group differences that served as endophenotype markers to distinguish the adolescents between TS and the normalized ones after CES.** ***Results:*** **Results showed that TS adolescents after CES treatment had stronger functional activity and connectivity in anterior cingulate cortex (ACC), caudate and posterior cingulate cortex while had weaker activity in supplementary motor area within the motor pathway compared with TS before CES.** ***Conclusion:*** **The results suggest that the functional activity and connectivity in motor pathway was suppressed while activities in the control portions within CSTC loop including ACC and caudate were increased in TS adolescents after CES compared with adolescents before CES.** ***Significance:*** **The normalization of the balance between motor and control portions of the CSTC circuit may result in the recovery of TS adolescents.**

***Index Terms*—Cranial electrotherapy stimulation (CES), independent component analysis (ICA), machine learning, resting-state fMRI (rs-fMRI), Tourette's syndrome (TS).**

I. Introduction

Tourette's syndrome (TS) is a neurological disorder characterized by repetitive, stereotyped, involuntary movements, and uncontrollable vocal tics. These symptoms typically appear before the age of 18 and the condition occurs in all ethnic groups with males affected three to four times more often than females [1]. The cortico-striato-thalamo-cortical (CSTC) circuit has been verified as an underlying neurobiological correlate of TS [2], [3]. High-resolution structural magnetic resonance imaging has shown that children and adult TS subjects displayed extensive brain abnormalities, including cortical thickness [4], [5] and changes in gray or white matter volumes in brain regions involved in prefrontal, sensorimotor, cingulate cortices and basal ganglia within CSTC circuit [6], [7]. Diffusion tensor imaging demonstrated that TS patients had decreased fractional anisotropy and increased radial diffusivity in the corticospinal tract, the corpus callosum, and long association fibre tracts compared with normal controls [8], [9]. In another study, the diffusion indices and tic severity of TS was reported to have a positive correlation in the amygdale, nucleus accumbens, globus pallidus, and putamen [10]. Functional neuroimaging studies have revealed brain activation and connection alterations in TS subjects during a variety of tics and nontics tasks [11], [12], including an increased functional interaction between primary motor cortex and supplementary motor cortex (SMA) during tics than intentional movements [13], different neuronal networks and connectivity patterns when performing increasingly demanding finger-tapping tasks [14], reduced activity in precentral gyrus, caudate and increased activity in medial frontal gyrus during finger-tapping task [15], frontal cortex and striatum during eye blinking inhabitation [16], altered connectivity of the ventral striatum in TS individuals with analyzing the functional coupling based on positron emission tomography [17]. Moreover, our previous study has investigated spontaneous and simulated tics in TS individuals with revealing that tics were caused by the combined effects of excessive activity in motor pathway and reduced activation in control portions of CSTC circuit [18], [19].

However, most studies have mainly examined task-specific neural anomalies in TS. It is likely that the core neural causes of TS are task independent. Several previous studies have also investigated resting-state functional magnetic resonance imaging (rs-fMRI) in TS subjects. One previous study computed the amplitude of low-frequency fluctuation (ALFF) and fractional ALFF (fALFF) of rs-fMRI data and found decreased ALFF/fALFF in posterior cingulate gyrus, anterior cingulated cortex, frontal cortex, and increased ALFF/fALFF in putamen and thalamus [20]. Another study investigated the functional

Manuscript received September 3, 2014; revised November 14, 2014; accepted December 13, 2014. Date of publication December 13, 2014; date of current version April 17, 2015. This work was supported by National Natural Science Foundation of China under Grant 11271232 and 61301253. Jianping Qiao and Shenhong Weng contributed equally to this work. *Asterisk indicates corresponding author.*

J. Qiao is with the College of Physics and Electronics, Shandong Normal University.

S. Weng is with the Department of Psychiatry, Wuhan University People Hospital.

P. Wang is with the School of Information Science and Engineering, Shandong University.

J. Long is with the School of Information Science and Engineering, Central South University.

*Z. Wang is with the Department of Psychiatry, Columbia University, New York, NY 10032 USA (email: wangz@nyspi.columbia.edu).

Color versions of one or more of the figures in this paper are available online at http://ieeexplore.ieee.org.

Digital Object Identifier 10.1109/TBME.2014.2385151

connectivity of the fronto-parietal control network and the cingulo-opercular control network with the predefined 39 regions of interest (ROIs) [21]. In addition, the temporal pattern of tic generation was demonstrated to follow the CSTC circuit by investigating tic-related activity and the underlying resting state networks [22]. But the functional connectivity and causality of the intrinsic CSTC neural circuits are still not examined.

We present the first study, as far as we know, to apply the independent component analysis (ICA) with hierarchical partner matching (HPM) algorithm following by granger causality analytical approaches used by Wang *et al*. [18], [23] to rs-fMRI data which were collected in patients with TS before and after cranial electrotherapy stimulation (CES) treatment to insight into the mechanism underlying this intervention strategy.

CES is a noninvasive therapeutic device that applies pulsed, alternating microcurrent ($<$1000 μA) transcutaneously to the head via electrodes placed on the earlobes, mastoid processes, zygomatic arches, or the maxillo-occipital junction. CES has been granted approval by the U.S. Food and Drug Administration since 1979 for the treatment of insomnia, depression, and anxiety, and it is commercially available for personal use. Compared with other established noninvasive stimulation techniques, such as transcranial magnetic stimulation or transcranial direct current stimulation, CES is relatively inexpensive, and it can be self-administered by patients with few side effects [24]. In the clinical applications of CES, it is recommended that patients can be prescribed a CES device to use at home with a regular 20- to 60-min treatment daily or every other day for the treatment of anxiety, depression, pain or insomnia [25]–[27]. CES effects are cumulative so those who do not respond initially may benefit when given daily treatments for one month or longer [28]. Previous neuroimaging studies have claimed that CES has beneficial effects in conditions such as anxiety, depression, insomnia, stress, and pain [26], [29]. A recent functional magnetic resonance imaging (fMRI) study tested 0.5- and 100-Hz stimulation on healthy controls, using blocks of 22 s "on" alternating with 22 s of baseline (device was "off"), suggesting that CES caused cortical brain deactivation in prefrontal and parietal regions [30]. Electroencephalographic studies showed that CES increased alpha activity (increased relaxation), decreased delta activity (reduced fatigue), and decreased beta activity (decreased ruminative thoughts) [26], [31]. In addition, CES has been found to induce changes in brain oscillation patterns, neurotransmitter, neurohormones and endorphin release, interruption of ongoing cortical activity, or secondary effects from peripheral nerve stimulation [32]. However, it remains unclear how the electrical current from CES may alter intrinsic brain activity and connectivity in clinical populations. In this study, we found that CES was effective in treating TS. We applied CES to the earlobes of TS patients. In this way, the current may initially stimulate afferent branches of cranial nerves. Then stimulation may be carried from branches of the facial, glossopharyngeal, and/or the vagus nerves to the brainstem, the thalamus, and finally the cortex [30]. We, therefore, hypothesized that CES could alter intrinsic brain activity and connectivity, which in turn improves the neuro dysfunction and leads to the normalization of intrinsic neural circuits governing TS.

ICA has been widely utilized for analyzing brain imaging data. ICA is intrinsically a multivariate method for blind separation of a composite signal into its constituent source signals. As a data-driven approach, ICA can be used to identify brain networks in resting-state fMRI besides task-related fMRI since it does not require a priori information about the source signals. Each independent component (IC) provides a grouping of brain regions that share the same response pattern, thus, providing a natural measure of functional connectivity. There has been several kinds of multisubject ICA analysis approaches (for a review, see [33]). We focus on the individual ICA approach that separates ICA analyses run on each subjects, followed by clustering to enable group since this approach can preserve the individuals unique spatial and temporal features.

In the present study, we examined blood oxygenation level dependent (BOLD) fluctuations and intrinsic brain functional connectivity based on resting-state functional MRI data. We applied ICA with HPM algorithm to identify ICs that were reproducible across individuals. We also calculated the granger causality index (GCI) [34], [35] as a measure of causal interactions among components of CSTC circuit that generate or control motor behaviors. We finally performed machine learning and pattern classification on ICs with significant group differences that can serve as endophenotype markers to distinguish the adolescents between TS before CES and normalized TS after CES.

II. Materials and Methods

A. CES Therapy

We used the CES device, called the alpha-stim stress control system in the clinical treatment, provided by the manufacturer, Electromedical Products International (Mineral Wells, Tex). The alpha-stim stress control system provides cranial electrical stimulation by generating bipolar, asymmetric rectangular waves with a frequency of 0.5 Hz and a current intensity that can be adjusted continuously to provide between 10 and 500 μA. At the beginning of the treatment, patient's earlobes were clipped by the electrodes, and the current was adjusted until the patient felt a mild tingling sensation and/or dizziness, at which point the current was reduced to just below the reported threshold of sensation. If the patient experienced no sensation, the investigator increased the current incrementally until the patient perceived a sensation and then reduced it slightly below that threshold. Once the current intensity was found, the patient was instructed to use it consistently throughout the duration of the 24 weeks of treatment.

The protocol of treatment was that patients took stimulation once a day with their parents' help at his or her place of residence when got in bed. The treatment duration was set to be 60 min each time. Patients could fall asleep during treatment.

B. Participants

We recruited 43 male or female right-handed patients (less than 12 years old) with a diagnosis of TS (according DSM-IV) in the study. All the patients were physical healthy and the IQ

examination were no less than 100. The patients were drug free for at least one month before recruited. The exclusion criteria include co-occurring anxiety and attention deficit hyperactivity disorder, current depression, current or previous history of psychosis.

Forty-two patients were completed 24-week treatment and one patient was dropped out one week after CES treatment for lack of efficacy. All the patients were encouraged to take fMRI scan before treatment and at the end of the treatment, but only eight patients completed both the treatment and scan since the fMRI scanning was optional for the patients. The safety screening form and informed consent form were approved by the Institutional Review Board of Wuhan University People Hospital. Parental consent was obtained from participants under age 18. The efficacy of CES was evaluated by Yale Global Tic Severity Scale (Y-GTSS), and the side effect was recorded according to patients' report.

C. Imaging Data Acquisition

Resting-state fMRI was performed on a 3T magnetic resonance unit (GE Signa Medical Systems, Twinspeed, Milwaukee) in the Renmin Hospital of Wuhan University. A birdcage head coil and restraining foam pads were used to minimize head motion. Functional data were acquired using a gradient-echo, $T2^*$-weighted echo-planar imaging with BOLD contrast pulse sequence. Thirty-two contiguous axial slices that covered the entire hemisphere and brainstem were acquired along the AC–PC plane, with a 64×64 matrix (repetition time $= 2000$ msec, echo time $= 30$ msec, field of view $= 24\,\mathrm{cm} \times 24\,\mathrm{cm}$, and slice thickness $= 4$ mm without a gap).

D. Data Analysis

1) Preprocessing: We preprocessed the fMRI data using the statistical parametric mapping software package SPM8 (Welcome Department of Imaging Neuroscience, London, United Kingdom; http://www.fil.ion.ucl.ac.uk/spm/) implemented in MATLAB 2012B. During the preprocessing procedures, the volumes were slice timing corrected, spatially realigned to correct for motion, normalized to Montreal Neurological Institute-coordinate system [36], resampled at $3\,\mathrm{mm} \times 3\,\mathrm{mm} \times 3\,\mathrm{mm}$, and spatially smoothed with an isotropic 8-mm full-width at half-maximum Gaussian kernel to remove spatial noise, and to compensate for residual variability in functional anatomy after spatial normalization and to facilitate application of Gaussian random field theory for adjusted statistical inference. The spatially smoothed functional data were high-pass filtered via a discrete cosine transform at a cutoff frequency of 1/128 Hz to remove low-frequency noise such as scanner drift.

2) ICA with HPM: First, we performed single-subject ICA for each subject after preprocessing. We used the principles of information criteria to determine the number of sets of ICs, *N*. We combined minimum description length [37], [38] and Akaike's information criterion [39] to estimate the lower and upper bounds, respectively, of the numbers of ICs to generate for each participant. Thus, these lower and upper bounds defined an interval for the number *N* of components to generate. For the TS datasets in this study, the interval was [20:130]. Unlike conventional ICA, in which only one set of ICs is generated (we term this "single-set ICA," or SS-ICA), we generated multiple sets of components for each participant, which we term "multiple-set ICA". For each participant, with an increment of ten over the interval [20:130], we used the FastICA algorithm to generate 12 sets of ICs, with each of the 12 sets containing either 20, 30, 40, 50, 60, 70, 80, 90, 100, 110, 120, or 130 components, respectively.

The fMRI data were decomposed to spatial ICs and mixing matrix by applying spatial ICA on each subject after and before CES. ICs represent brain functional activity and connectivity. The corresponding column of each IC is time course, which represents the time variety of brain function network.

Second, we applied HPM algorithm to identify the reliable components that are significantly reproducible among different subject. We define a *family* of ICs as referring to the set of all ICs for a single scanning run. In this study, we had data from eight participants in the TS group before and after CES treatment, yielding a total of $8 + 8 = 16$ different families. For each of the 16 families, we generated 12 sets of ICs, with each of the 12 sets containing either 20, 30, 40, 50, 60, 70, 80, 90, 100, 110, 120, or 130 components, as described earlier. In addition, we have demonstrated previously that assessing whether a matching is bidirectional is a useful and valid way to test whether an IC is reproducible between families [23], which terms the Partner Matching algorithm. In detail, given a component *i* from family A, we calculate indices of spatial similarity between IC *i* from family A and each IC in family B. We use Tanimoto Distance to quantify this spatial similarity between components [23]. We then select the component from family B, say component *j*, that is determined to have the maximum similarity index to component *i* among all the components of family B. After that, we calculate all the similarity indices between component *j* from family B and each of the components in family A. We then select the component from family A, say component *k*, that is determined to have the maximum similarity index to component *j* among all the components of family A. If $k = i$, then the matching is bidirectional, and we consider this component in family A and this component in family B to be partner matched. We repeat this procedure to find all pairs of components that are bidirectionally matched between families A and B. Then, we apply this algorithm to identify matching components across multiple families. We call a collection of components that match across families a *cluster*. For example, a cluster may contain component *i* of family A, component *j* of family B, component *m* of family C, etc., all of which are matched to one another according to the partner matching procedure described earlier. Therefore, each of these clusters contains the information of component correspondences between families.

There are two steps in the HPM algorithm. In the first step, we used Tanimoto distance to quantify the spatial similarity between components and only bidirectional matching ICs were identified as matching components cross multiple subjects. These components that were identified as being significantly similar to one another in their spatial configuration formed a cluster. We then performed one-sample *t* test on the *z* score

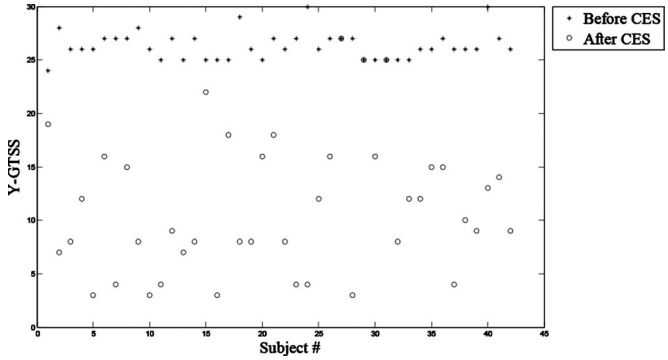

Fig. 1. Y-GTSS scores of the 42 patients before and after CES treatment. The horizontal axis shows the subject number from 1 to 42. The first eight subjects are the eight patients that completed the fMRI sessions. The vertical axis shows the Y-GTSS score. The star stands for the Y-GTSS score of the subjects before CES. The circle stands for the Y-GTSS score of the subjects after CES.

maps of ICs within each cluster to obtain the map of significant voxels for that cluster. The cluster map represented a spatial pattern that tends to be present across subjects. In the second step, we applied partner matching to the cluster maps to identify corresponding clusters across the different sets. The clusters with the highest Cronbach's Alpha were selected as optimal clusters. Each cluster means a pattern that has one or more brain regions. The cluster of artifactual ICs were identified visually and only the meaningful clusters be used for the following analysis. We finally computed the GCI to assess causal influence between these brain regions by extracting the time course of each IC within each pattern.

3) Group Differences Between Before and After CES Treatment: The z score maps of reproducible ICs were entered into group-level random-effect analysis. For each cluster, we entered z score maps of ICs into the second-level paired t test model implemented in SPM8 factorial module to detect a random effect of the group difference of the functional connectivity between the TS adolescents after and before CES. The second-level analysis identified significant group differences in ROIs within CSTC circuit. These regions were selected for the pattern recognition analyses.

4) Machine Learning: By extracting the eigenvectors from each subject's individual z score maps of ICs, the time series of within each of the ROIs that had significant group differences were defined as the features vectors. We performed pattern recognition using two methods: support vector machine (SVM) and the maximum uncertainty linear discriminant analysis (MLDA) [40] with cross validation to classify the TS patients before and after CES and cross verify the detected normalized functional activity and connectivity results. The support vector optimization problem can be solved analytically only when the number of training data is very small [41]. The MLDA method was also suitable in the situation of small samples [40]. In addition, fivefold cross validation and leave-one-out cross validation method were used to quantify the performance of SVM classifier. The classification accuracy was calculated by averaging 1000 cross validation trials with randomly selected subsets. Therefore, the sample size in this study is not large but remains acceptable for binary classification. Importantly, the accurate classification was able to cross verify the features that detected by ICA and identify the difference of the TS patients between before and after the CES.

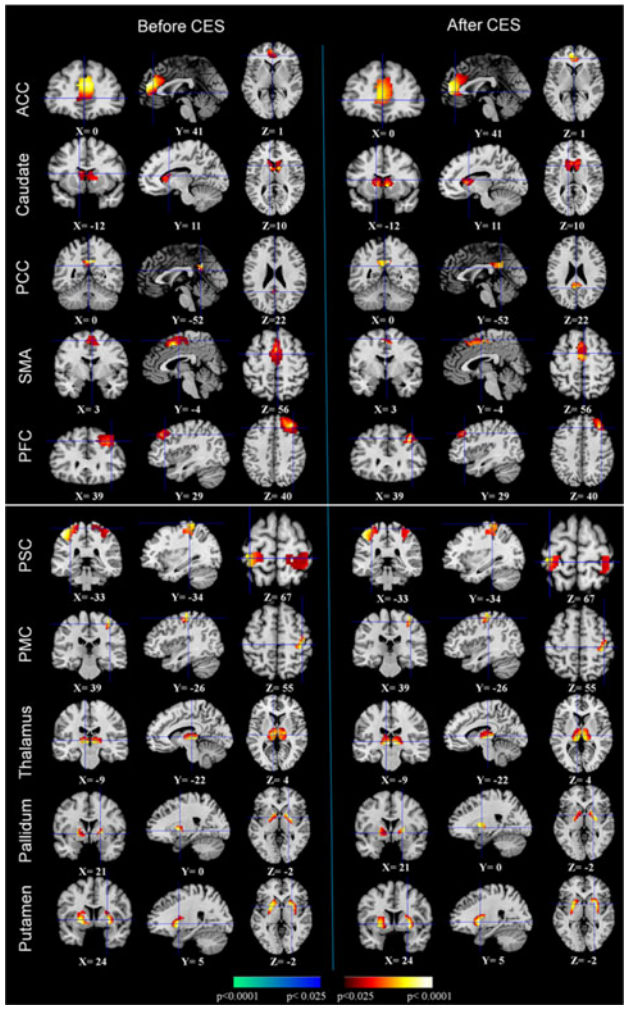

Fig. 2. Activity in each of the ten clusters of reproducible independent components. The first set of three columns displays the random-effect group activity maps detected from the eight Tourette's syndrome patients before CES treatment. The first column is a coronal view, the second is a sagittal view, and the third is an axial view. The second set of three columns displays the group activity maps detected from the eight Tourette's syndrome patients after CES treatment. Each row in the first and second set of columns displays one group activity map that was generated by applying a one-sample t test to one of the ten clusters of independent components. Any two group activity maps within the same row across the first and second columns are significantly similar to one another in their spatial configurations. ACC = anterior cingulate cortex; PCC = posterior cingulate cortex; SMA = supplementary motor cortex; PFC = prefrontal cortex; PSC = primary somatosensory cortex; PMC = primary motor cortex.

III. Results

A. Clinical Results

The mean age of the 42 patients that have completed the treatment was 95.90 ± 23.48 months. The duration of TS was 21.12 ± 9.11 months. The score of Y-GTSS was 26.33 ± 1.32 before CES. The total score of Y-GTSS was 11.36 ± 6.44 after 24-week treatment of CES. We applied two-sample t test to assess the group difference in Y-GTSS scores of patients

between before and after CES. The 42 patients after CES had significantly lower Y-GTSS scores than the ones before CES ($p = 8.14e-25$, $t = -14.77$, after CES versus before CES).

The mean age of the eight patients that have completed fMRI scan was 105.88 ± 23.76 months. The duration of TS was 22.50 ± 4.24 months. The score of Y-GTSS was 26.38 ± 1.19 before CES. The total score of Y-GTSS was 10.50 ± 5.88 after 24-week treatment of CES. The eight patients after CES had significantly lower Y-GTSS scores than the ones before CES ($p = 2.94e-06$, $t = -7.49$, after CES versus before CES). All the eight patients with fMRI were responsive to treatment and three of the 42 patients after CES had the same Y-GTSS scores as the ones before CES. There was no patient that had increased Y-GTSS scores after CES among all 42 patients (see Fig. 1).

We compared the eight patients that had completed MRI scan and the total 42 patients that had completed the trial. There was no statistical significant difference in age, duration of TS, and score of TS between them. There were four headaches and two insomnia reports. All the events were released without special treatment during the trial.

B. Reproducible ICs

We performed spatial ICA to generate twelve sets of ICs, with each of the twelve sets containing either 20, 30, 40, 50, 60, 70, 80, 90, 100, 110, 120, or 130 components, for each TS patient after and before CES. We then applied HPM method to the 12 sets of components to identify ten significantly reproducible clusters of ICs in their spatial patterns across patients. One-sample *t* test was performed on the ten clusters of ICs for after and before CES groups, respectively, to generate ten ICs maps, which represent brain functional activity and connectivity (see Fig. 2).

C. Group Difference in Resting-State Functional Connectivity Patterns Before and After CES

The ten reproducible ICs of before and after TS subjects were compared in a second-level random-effects analysis by using paired two tailed *t* test. Compared with TS patients before CES, TS patients after CES showed significantly lower intrinsic functional connectivity in anterior cingulate cortex (ACC), caudate and posterior cingulate cortex (PCC). Meanwhile, TS patients after CES showed significantly greater intrinsic functional connectivity in the SMA, prefrontal cortex (PFC) and primary somatosensory cortex (PSC) (see Fig. 3 and Table I). We used a combination of p value of 0.01 and cluster extent threshold of 30 voxels (determined by Monte Carlo simulation) to correct for multiple comparison. We computed the correlations between the activity of the six regions and the score difference of Y-GTSS (Y-GTSS of after CES minus Y-GTSS of before CES). Activity in SMA, PFC, and PSC correlated positively with the difference of Y-GTSS score, while activity in ACC, caudate, and PCC correlated inversely with the score difference. Only neural activity in SMA correlated significantly with the score difference ($r = 0.71$, $p < 0.05$).

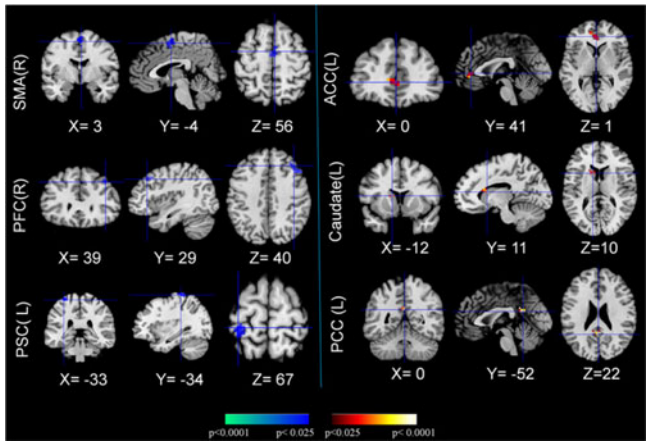

Fig. 3. Normalization of brain activity with CES treatment (TS patients after CES versus TS patients before CES). The two sets of three columns display *t* contrast maps comparing the group activity maps from the Tourette's syndrome patients after CES and before CES. The images show that relative to Tourette's syndrome patients before CES, Tourette's syndrome patients after CES had weaker activity (as evidenced by the color blue, the first sets of three columns) in the SMA, PFC, PSC, while had stronger activity (as evidenced by the color red, the second sets of three columns) in the ACC, caudate, and PCC.

D. Granger Causality Interactions

We computed two types of granger causality indices between the time courses of the selected reproducible ten ICs for each participant. One is influence of regions A on B, the other is influence of regions A on B through thalamus. That is because the top-down circuit from cortex to basal ganglia is direct, while the bottom-up circuit from basal ganglia to cortex via the thalamus. The TS patients after CES group showed stronger causal influences compared with before CES group in the connections from PFC to caudate (0.19 ± 0.06 versus 0.09 ± 0.06, $t = 3.60$, $p = 0.0029$), from PFC to ACC (0.15 ± 0.09 versus 0.04 ± 0.03, $t = 3.38$, $p = 0.0045$), from the caudate to PFC via the thalamus (0.16 ± 0.14 versus 0.05 ± 0.04, $t = 2.23$, $p = 0.0428$), while the TS patients after CES group showed weaker causal influences in the connections from SMA to PMC (0.07 ± 0.05 versus 0.13 ± 0.06, $t = -2.16$, $p = 0.0484$), from pallidum to SMA via the thalamus (0.04 ± 0.02 versus 0.17 ± 0.15, $t = -2.27$, $p = 0.0393$) (see Table II).

E. Machine Learning Results

Using the activity within the ACC, caudate, PCC, SMA, PFC, and PSC resulted from group difference in functional connectivity patterns before and after CES, we performed a machine learning algorithm based on SVM to classify the TS patients before and after CES treatment, yielding an average accuracy of 84.28% with five-fold cross validation method and 87.60% with leave-one-out cross validation method. Additionally, we also performed classification using the MLDA-based classifier with leave-one-out cross validation, which achieved a classification accuracy of 87.50% with a sensitivity of 86.23% and a specificity of 91.47%. The classification contributions as shown in Table I were obtained by the coefficients of the discrimination hyperplane that measures the weights of these features to the classification.

TABLE I
LOCATION AND COMPARISONS OF INDEPENDENT COMPONENT MAPS BETWEEN TS PATIENTS AFTER AND BEFORE CES

Brain Areas	Location		Peak location			T	Classification
	Side	BA	x	y	z	statistic	contribution
TS patients after versus before (positive)							
ACC	L	24	0	41	1	+4.08	0.4568
Caudate	L	NA	− 12	11	10	+3.40	0.3022
PCC	L	31	0	− 52	22	+3.33	0.2801
TS patients after versus before (negative)							
SMA	L	6	− 3	− 7	58	− 3.93	0.3980
	R	6	3	− 4	56	− 3.96	0.6412
PFC	R	46	39	29	40	− 4.22	0.4750
PSC	L	1	− 33	− 34	67	− 4.07	0.3875

NA = Not applicable.
All coordinates are in the Montreal Neurological Institute ICBM 152 template.

TABLE II
COMPARISONS OF GRANGER CAUSALITY INDICES OF THE INTERREGIONAL CONNECTIONS OF THE REPRODUCIBLE INDEPENDENT COMPONENTS

	TS patients after CES	TS patients before CES	TS patients After versus Before
PFC → SMA	$0.14 \pm 0.08, \mathrm{p} = 1.70\mathrm{E}-03$	$0.10 \pm 0.04, \mathrm{p} = 1.17\mathrm{E}-04$	$\mathrm{t} = 1.19, \mathrm{p} = 2.55\mathrm{E}-01$
PFC → Caudate	$0.19 \pm 0.06, \mathrm{p} = 5.51\mathrm{E}-05$	$0.09 \pm 0.06, \mathrm{p} = 4.50\mathrm{E}-03$	$\mathbf{t = 3.60, p = 2.90E-03}$
PFC → ACC	$0.15 \pm 0.09, \mathrm{p} = 1.81\mathrm{E}-03$	$0.04 \pm 0.03, \mathrm{p} = 4.36\mathrm{E}-03$	$\mathbf{t = 3.38, p = 4.50E-03}$
SMA → PMC	$0.07 \pm 0.05, \mathrm{p} = 7.12\mathrm{E}-03$	$0.13 \pm 0.06, \mathrm{p} = 2.74\mathrm{E}-04$	$\mathbf{t = -2.16, p = 4.84E-02}$
PSC → PMC	$0.14 \pm 0.13, \mathrm{p} = 1.52\mathrm{E}-03$	$0.19 \pm 0.13, \mathrm{p} = 4.93\mathrm{E}-03$	$\mathrm{t} = -0.70, \mathrm{p} = 4.97\mathrm{E}-01$
PMC → Putamen	$0.05 \pm 0.04, \mathrm{p} = 2.04\mathrm{E}-03$	$0.06 \pm 0.08, \mathrm{p} = 6.94\mathrm{E}-03$	$\mathrm{t} = -0.26, \mathrm{p} = 7.95\mathrm{E}-01$
PSC → Putamen	$0.08 \pm 0.05, \mathrm{p} = 4.32\mathrm{E}-03$	$0.09 \pm 0.08, \mathrm{p} = 1.42\mathrm{E}-03$	$\mathrm{t} = -0.36, \mathrm{p} = 7.27\mathrm{E}-01$
Pallidum → SMA via Thalamus	$0.04 \pm 0.02, \mathrm{p} = 2.80\mathrm{E}-03$	$0.17 \pm 0.15, \mathrm{p} = 1.63\mathrm{E}-03$	$\mathbf{t = -2.27, p = 3.93E-02}$
Pallidum → PFC via Thalamus	$0.19 \pm 0.18, \mathrm{p} = 1.95\mathrm{E}-03$	$0.15 \pm 0.13, \mathrm{p} = 1.49\mathrm{E}-03$	$\mathrm{t} = 0.46, \mathrm{p} = 6.52\mathrm{E}-01$
Pallidum → PMC via Thalamus	$0.10 \pm 0.08, \mathrm{p} = 1.38\mathrm{E}-03$	$0.13 \pm 0.11, \mathrm{p} = 1.13\mathrm{E}-03$	$\mathrm{t} = -0.72, \mathrm{p} = 4.81\mathrm{E}-01$
Pallidum → PSC via Thalamus	$0.11 \pm 0.07, \mathrm{p} = 2.22\mathrm{E}-03$	$0.14 \pm 0.07, \mathrm{p} = 6.33\mathrm{E}-04$	$\mathrm{t} = -0.83, \mathrm{p} = 4.23\mathrm{E}-01$
Caudate → PFC via Thalamus	$0.16 \pm 0.14, \mathrm{p} = 1.13\mathrm{E}-03$	$0.05 \pm 0.04, \mathrm{p} = 4.91\mathrm{E}-03$	$\mathbf{t = 2.23, p = 4.28E-02}$

The data in each cell in the second and third column represent the mean±std of the GCI. We used two-sample *t* test to compare the GCIs of TS between after and before CES groups. The bold in the last column indicates that the comparisons are significant ($\mathrm{p} < 0.05$, uncorrected). X → Y via Thalamus represents the connectivity between X and Y via the thalamus.

IV. DISCUSSION AND CONCLUSION

In the present study, we applied HPM-ICA, granger causality as well as pattern recognition methods based on rs-fMRI data to investigate and cross verify the normalization in intrinsic brain functional activity and connectivity between TS patients before and after CES therapy. We found that TS patients after CES exhibited altered spontaneous functional connectivity in brain areas within CSTC circuit involved in motor generation or control, including SMA, caudate, PFC, ACC, and default mode network (DMN), primary in PCC. The functional activity and connectivity in motor pathway was suppressed, while activations in the control portions of CSTC loop were increased in the TS patients after CES compared with ones before CES. The normalization of the balance between motor and control portions of the CSTC circuit may result in the recovery of TS patients. To our knowledge, this is the first study to apply the HPM-ICA and granger causality analytical approaches to rs-fMRI data with TS patients before and after CES treatment. From the perspective of neurophysiology, we concluded that the intervention of CES was able to improve the brain neuro dysfunction and had the obvious promotion effect on TS for their brain function improvement, which translates the changes of the intrinsic connectivity networks to therapeutic mechanisms of action and provides an objective experimental basis for its application in TS.

We found significantly greater activity in ACC and caudate in the TS patients after CES than before CES. This finding is consistent with our previous reports of functional anomalies or disconnections in this region in TS patients [18]. One DTI study demonstrated that cortical regions as well as limbic structures take part in the modulation of tics [9]. Other studies have also shown decreased fALFF in ACC in TS adolescents based on rs-fMRI [20], increased activity in ACC during tic suppression [11], reduced caudate volume both in TS adults and adolescents [42], [43]. ACC plays an important role in the engagement of cognitive control [44], [45] that together with caudate represent the control portions of the CSTC circuit. Tics are caused by the combined effects of excessive activity in motor pathway and reduced activity in control portions of CSTC circuits [18]. Therefore, increased pathological intrinsic functional activity and connectivity in ACC and caudate represented the normalized engagement of control portions of CSTC circuit.

The TS patients that after CES group had weaker intrinsic neural activity than ones that before CES group within the supplementary motor area (SMA). In patients with TS disease, it has been shown that brain regions in the motor pathway of CSTC circuit, including SMA, premotor area, primary motor

area, putamen, pallidum and substantia nigra, exhibited excessive activity compared with normal controls [18]. Another fMRI study reported that activation and functional connectivity of motor network including frontal, parietal, and subcortical areas were altered in adult TS patients as compared to controls during performance of tasks such as finger tapping [14]. We did not detect significant differences in basal ganglia and thalamus by comparing the reliable ICs of TS patients before and after CES groups. This result is consistent with previous DTI reports, which only reported the correlation between diffusion parameters and measures of tic severity within the TS group but did not find significant differences in the diffusion indices of basal ganglia and the thalamus between TS patients and controls [10]. However, we did find that causal influence of the putamen on SMA via thalamus was weaker in the TS patients after CES than ones before CES. Previous researches demonstrate that SMA is responsible to trigger motor response or anticipate that a movement is going to occur [46], [47]. Moreover, SMA has been shown to play an importance role in tics generation no matter in resting state or task-related fMRI TS studies [13], [22]. Abnormal activation of motor cortex via basal ganglia thalamocortical circuits would cause relatively simple tics. Abnormal activation of SMA as well as premotor and cingulate motor areas would cause complex tics [48]. Therefore, the weaker activity in SMA and GCI from the putamen to SMA via thalamus suggests the normalization of the motor pathway in CSTC circuit.

We detected the DMN in the reproducible ICs and then compared the intrinsic functional activity between TS patients after and before CES. We found increased functional activity in PCC in TS patients after CES than ones before CES. The DMN that mainly includes the PCC, medial prefrontal cortex, bilateral inferior parietal lobes, and the medial temporal lobe is typically deactivate during cognitive tasks [49]. Particularly, PCC plays a pivotal role in the DMN [50] which has also been strongly implicated as a key part of several intrinsic cognitive control networks [51]. Some previous studies revealed the decreased ALFF in PCC in TS adolescents [20] based on rs-fMRI, attenuated deactivations with age in PCC in TS adults during a stroop task [52]. The abnormal pattern of deactivation or low-frequency fluctuation may reflect the inability to maintain efficient control of the PCC/DMN function [53]. Therefore, our finding of increased functional activity and connectivity in PCC suggests the normalization of functional deficits associated with impaired motor inhibition.

Computer modeling predictions using a highly detailed anatomical model has shown that CES induced significant currents in cortical and subcortical structures [54]. Moreover, CES stimulation has been investigated to alter cortical activation and brain connectivity in the DMN [30]. Convergent evidence has shown that CES caused the alpha band mean or median frequency to shift downward [55], [56]. Meanwhile, the alpha band conveyed information about the BOLD signal [57]. Therefore, the observation of altered BOLD signal was associated with CES therapy. In this way, CES may alter brain oscillation patterns since the oscillating current from CES may interrupt nervous system function, resulting in deactivation of cortical activity [30]. The normalization of TS patients after CES may due to the changes in brain activity and intrinsic connectivity networks in line with evidence that stimulation interferes with oscillatory brain activity and is associated with reduction of brain wave frequencies (mean alpha power) [30].

Furthermore, SVM and MLDA were used to create classifier models that distinguished TS patients before CES from TS patients after CES treatment, which attained 87.6% and 87.5% classification accuracy with leave-one-out cross validation, respectively. The high classification accuracy suggested that the intrinsic functional connectivity in brain regions within CSTC circuit could truly differentiate the two groups and cross verify the detected normalized connectivity, which can be used as endophenotype to classify the TS patients before and after CES.

Several limitations of the present study should be noted. First, the sample size in this study was not large. However, we calculated the classification accuracy by averaging 1,000 cross validation trials with randomly selected subsets, which cross verify the findings of the normalized functional connectivity. The future work should be done on a larger training sample, which may lead to higher classification accuracy. Second, considering no risk to try CES treatment, the patients who had tried all the other treatments with no effective outcome voluntarily participated in the test with a sole purpose to reduce their tic symptoms and, thus, were very eager to see the effective outcome of new treatment using CES. Therefore, this was a clinical sample and there was not a "sham" stimulation group in this study. We compared the group difference between patients before and after CES and achieved high-classification accuracy, suggesting that the findings from patients before and after CES provide important insights into the neuroscience of TS normalization after CES, similar studies consisting of an active CES group, a control group and a "sham" treatment group are needed to do further more relevant analysis including the group comparison and classification analysis. Third, different TS individuals may have different responses to the scanner noise of fMRI which may lead to change of brain function. It will be necessary to replicate these results with silent techniques such as EEG. Finally, the individual ICA method has the advantage of getting unique spatial and temporal features, but ICs are not necessary uncompounded in the same way since the noisy maybe different for each participant.

REFERENCES

[1] D. Martino *et al.*, "An introduction to the clinical phenomenology of Tourette syndrome," *Int. Rev. Neurobiol.*, vol. 112, pp. 1–33, 2013.
[2] J. W. Mink, "Neurobiology of basal ganglia and Tourette syndrome: Basal ganglia circuits and thalamocortical outputs," *Adv. Neurol.*, vol. 99, pp. 89–98, 2006.
[3] B. Draganski *et al.*, "Multispectral brain morphometry in Tourette syndrome persisting into adulthood," *Brain*, vol. 133, no. Pt 12, pp. 3661–3675, Dec. 2010.
[4] E. R. Sowell *et al.*, "Thinning of sensorimotor cortices in children with Tourette syndrome," *Nature Neurosci*, vol. 11, no. 6, pp. 637–639, Jun. 2008.
[5] C. Fahim *et al.*, "Somatosensory-motor bodily representation cortical thinning in Tourette: Effects of tic severity, age and gender," *Cortex*, vol. 46, no. 6, pp. 750–760, Jun. 2010.
[6] V. Roessner *et al.*, "Increased putamen and callosal motor subregion in treatment-naive boys with Tourette syndrome indicates changes in the

bihemispheric motor network," *J. Child Psychol. Psychiatry*, vol. 52, no. 3, pp. 306–314, Mar. 2011.
[7] A. G. Ludolph *et al.*, "Grey-matter abnormalities in boys with Tourette syndrome: Magnetic resonance imaging study using optimised voxel-based morphometry," *Brain J. Psychiatry*, vol. 188, pp. 484–485, May 2006.
[8] A. E. Cavanna *et al.*, "Corpus callosum abnormalities in Tourette syndrome: An MRI-DTI study of monozygotic twins," *J. Neurol. Neurosurg Psychiatry*, vol. 81, no. 5, pp. 533–5, May 2010.
[9] I. Neuner *et al.*, "White-matter abnormalities in Tourette syndrome extend beyond motor pathways," *Neuroimage*, vol. 51, no. 3, pp. 1184–1193, Jul. 1, 2010.
[10] I. Neuner *et al.*, "Microstructure assessment of grey matter nuclei in adult Tourette patients by diffusion tensor imaging," *Neurosci. Lett.*, vol. 487, no. 1, pp. 22–26, Jan. 3, 2011.
[11] B. S. Peterson *et al.*, "A functional magnetic resonance imaging study of tic suppression in Tourette syndrome," *Arch. Gen .Psychiatry*, vol. 55, no. 4, pp. 326–333, Apr. 1998.
[12] S. Bohlhalter *et al.*, "Neural correlates of tic generation in Tourette syndrome: An event-related functional MRI study," *Brain*, vol. 129, no. Pt 8, pp. 2029–2037, Aug. 2006.
[13] M. Hampson *et al.*, "Brain areas coactivating with motor cortex during chronic motor tics and intentional movements," *Biol. Psychiatry*, vol. 65, no. 7, pp. 594–599, Apr 1, 2009.
[14] C. J. Werner *et al.*, "Altered motor network activation and functional connectivity in adult Tourette's syndrome," *Human Brain Mapping*, vol. 32, no. 11, pp. 2014–2026, Nov. 2011.
[15] V. Roessner *et al.*, "Altered motor network recruitment during finger tapping in boys with Tourette syndrome," *Hum Brain Mapping*, vol. 33, no. 3, pp. 666–675, Mar. 2012.
[16] L. Mazzone *et al.*, "An FMRI study of frontostriatal circuits during the inhibition of eye blinking in persons with Tourette syndrome," *Amer. J. Psychiatry*, vol. 167, no. 3, pp. 341–349, Mar. 2010.
[17] K. J. Jeffries *et al.*, "The functional neuroanatomy of Tourette's syndrome: An FDG PET study III: functional coupling of regional cerebral metabolic rates," *Neuropsychopharmacology*, vol. 27, no. 1, pp. 92–104, Jul. 2002.
[18] Z. Wang *et al.*, "The neural circuits that generate tics in Tourette's syndrome," *Amer. J. Psychiatry*, vol. 168, no. 12, pp. 1326–1337, Dec. 2011.
[19] D. J. Greene and B. L. Schlaggar, "Insights for treatment in Tourette syndrome from fMRI," *Trends Cogn. Sci.*, vol. 16, no. 1, pp. 15–6, Jan. 2012.
[20] Y. Cui *et al.*, "Abnormal baseline brain activity in drug-naive patients with Tourette syndrome: A resting-state fMRI study," *Front Hum Neurosci*, vol. 7, p. 913, 2014.
[21] J. A. Church *et al.*, "Control networks in paediatric Tourette syndrome show immature and anomalous patterns of functional connectivity," *Brain*, vol. 132, no. Pt 1, pp. 225–238, Jan. 2009.
[22] I. Neuner *et al.*, "Imaging the where and when of tic generation and resting state networks in adult Tourette patients," *Front Hum Neurosci*, vol. 8, p. 362, 2014.
[23] Z. Wang and B. S. Peterson, "Partner-matching for the automated identification of reproducible ICA components from fMRI datasets: algorithm and validation," *Human Brain Mapping*, vol. 29, no. 8, pp. 875–893, Aug. 2008.
[24] A. Bystritsky *et al.*, "A pilot study of cranial electrotherapy stimulation for generalized anxiety disorder," *J. Clin. Psychiatry*, vol. 69, no. 3, pp. 412–417, Mar. 2008.
[25] S. H. Lee *et al.*, "Effects of cranial electrotherapy stimulation on preoperative anxiety, pain and endocrine response," *J. Int. Med. Res.*, vol. 41, no. 6, pp. 1788–1795, Dec. 2013.
[26] D. L. Kirsch and F. Nichols, "Cranial electrotherapy stimulation for treatment of anxiety, depression, and insomnia," *Psychiatr Clin. North Amer.*, vol. 36, no. 1, pp. 169–176, Mar. 2013.
[27] T. H. Barclay and R. D. Barclay, "A clinical trial of cranial electrotherapy stimulation for anxiety and comorbid depression," *J. Affective Disorders*, vol. 164, pp. 171–177, Aug. 2014.
[28] J. T. Holubec, "Cumulative response from cranial electrotherapy stimulation (CES) for chronic pain," *Practical Pain Manag.*, vol. 9, no. 9, pp. 80–83, 2009.
[29] M. F. Gilula and P. R. Barach, "Cranial electrotherapy stimulation: A safe neuromedical treatment for anxiety, depression, or insomnia," *South Med. J.*, vol. 97, no. 12, pp. 1269–1270, Dec. 2004.
[30] J. D. Feusner *et al.*, "Effects of cranial electrotherapy stimulation on resting state brain activity," *Brain Behav.*, vol. 2, no. 3, pp. 211–220, May 2012.
[31] R. Kennerly, "QEEG analysis of cranial electrotherapy: A pilot study," *J. Neurotherapy*, vol. 8, no. 2, pp. 112–113, 2004.
[32] S. Zaghi *et al.*, "Noninvasive brain stimulation with low-intensity electrical currents: Putative mechanisms of action for direct and alternating current stimulation," *Neuroscientist*, vol. 16, no. 3, pp. 285–307, Jun. 2010.
[33] V. D. Calhoun *et al.*, "A review of group ICA for fMRI data and ICA for joint inference of imaging, genetic, and ERP data," *Neuroimage*, vol. 45, no. Suppl. 1, pp. S163–S172, Mar. 2009.
[34] C. W. J. Granger, "Investigating causal relations by econometric models and cross-spectral methods," *Econometrica*, vol. 37, no. 3, pp. 424–438, Aug. 1969.
[35] Y. Chen *et al.*, "Analyzing multiple nonlinear time series with extended Granger causality," *Phys. Lett. A*, vol. 324, no. 1, pp. 26–35, Apr. 2004.
[36] K. J. Friston *et al.*, "Spatial registration and normalization of images," *Human Brain Mapping*, vol. 3, no. 3, pp. 165–189, 1995.
[37] V. D. Calhoun *et al.*, "A method for making group inferences from functional MRI data using independent component analysis," *Human Brain Mapping*, vol. 14, no. 3, pp. 140–151, Nov. 2001.
[38] J. Rissanen, "A universal prior for integers and estimation by minimum description length," *Annals Statist.*, vol. 11, no. 2, pp. 416–431, Jun. 1983.
[39] H. Akaike, "A new look at the statistical model identification," *IEEE Trans. Automat. Control*, vol. AC-19, no. 6, pp. 716–723, Dec. 1974
[40] Z. Dai *et al.*, "Discriminative analysis of early Alzheimer's disease using multi-modal imaging and multi-level characterization with multi-classifier (M3)," *Neuroimage*, vol. 59, no. 3, pp. 2187–2195, Feb. 1, 2012.
[41] C. J. C. Burges, "A tutorial on support vector machines for pattern recognition," *Data Mining Knowl. Discovery*, vol. 2, no. 2, pp. 121–167, Jun. 1998.
[42] B. S. Peterson *et al.*, "Basal ganglia volumes in patients with Gilles de la Tourette syndrome," *Arch. Gen. Psychiatry*, vol. 60, no. 4, pp. 415–424, Apr. 2003.
[43] M. I. Makki *et al.*, "Microstructural abnormalities of striatum and thalamus in children with Tourette syndrome," *Mov. Disord.*, vol. 23, no. 16, pp. 2349–2356, Dec. 15, 2008.
[44] J. G. Kerns *et al.*, "Anterior cingulate conflict monitoring and adjustments in control," *Science*, vol. 303, no. 5660, pp. 1023–1026, Feb. 13, 2004.
[45] M. Botvinick *et al.*, "Conflict monitoring versus selection-for-action in anterior cingulate cortex," *Nature*, vol. 402, no. 6758, pp. 179–181, Nov. 11, 1999.
[46] M. Erdler *et al.*, "Dissociation of supplementary motor area and primary motor cortex in human subjects when comparing index and little finger movements with functional magnetic resonance imaging," *Neurosci. Lett.*, vol. 313, no. 1–2, pp. 5–8, Nov. 2, 2001.
[47] N. Arai *et al.*, "Effective connectivity between human supplementary motor area and primary motor cortex: A paired-coil TMS study," *Exp. Brain Res.*, vol. 220, no. 1, pp. 79–87, Jul. 2012.
[48] J. W. Mink, "Basal ganglia dysfunction in Tourette's syndrome: A new hypothesis," *Pediatr. Neurol.*, vol. 25, no. 3, pp. 190–198, Sep. 2001.
[49] R. L. Buckner *et al.*, "The brain's default network: Anatomy, function, and relevance to disease," *Ann. NY Acad. Sci.*, vol. 1124, pp. 1–38, Mar. 2008.
[50] P. Fransson and G. Marrelec, "The precuneus/posterior cingulate cortex plays a pivotal role in the default mode network: Evidence from a partial correlation network analysis," *Neuroimage*, vol. 42, no. 3, pp. 1178–1184, Sep. 1, 2008.
[51] R. Leech and D. J. Sharp, "The role of the posterior cingulate cortex in cognition and disease," *Brain*, vol. 137, no. Pt 1, pp. 12–32, Jan. 2014.
[52] R. Marsh *et al.*, "A developmental fMRI study of self-regulatory control in Tourette's syndrome," *Amer. J. Psychiatry*, vol. 164, no. 6, pp. 955–966, Jun. 2007.
[53] R. N. Spreng and D. L. Schacter, "Default network modulation and large-scale network interactivity in healthy young and old adults," *Cereb Cortex*, vol. 22, no. 11, pp. 2610–2621, Nov. 2012.
[54] A. Datta *et al.*, "Cranial electrotherapy stimulation and transcranial pulsed current stimulation: A computer based high-resolution modeling study," *Neuroimage*, vol. 65, pp. 280–287, Jan. 15, 2013.
[55] T. Itil *et al.*, "Quantitative EEG analysis of electrosleep using analog frequency analyzer and digital computer methods," *Dis. Nerv. Syst.*, vol. 33, no. 6, pp. 376–381, Jun. 1972.
[56] M. J. Schroeder and R. E. Barr, "Quantitative analysis of the electroencephalogram during cranial electrotherapy stimulation," *Clin. Neurophysiol.*, vol. 112, no. 11, pp. 2075–2083, Nov. 2001.
[57] C. Magri *et al.*, "The amplitude and timing of the BOLD signal reflects the relationship between local field potential power at different frequencies," *J. Neurosci.*, vol. 32, no. 4, pp. 1395–1407, Jan. 25, 2012.

Jianping Qiao received the B.S. degree in electronic engineering from the University of Petroleum, Dongying, China, in 2003, and the Ph.D. degree in communication and information system from Shandong University, Jinan, China, in 2008.

She is currently a Lecturer at College of Physics and Electronics, Shandong Normal University, Jinan, China. Her current research interests include MRI image processing and analysis, brain structure and function analysis, and brain network analysis.

Shenhong Weng received the M.D. degree from Medical School of Wuhan University, Wuhan, China, in 2008.

He is currently an Associate Chief Physician and an Associate Professor at Renmin Hospital of Wuhan University, Wuhan, China. His current research interests include transcranial electrical stimulation or transcranial magnetic stimulation on mental disorders.

Pengwei Wang (M'09) received the B.S. degree from Xi'an Jiaotong University, Xi'an, China, in 2000, and the Ph.D. degree in information engineering from the University of Science and Technology of China, Hefei, China, in 2007.

He was a Postdoctoral Fellow at the Columbia University Medical Center, New York, NY, USA, in 2009. He is currently a Lecturer at the School of Information Science and Engineering, Shandong University, Jinan, China. His research has been concerned with biomedical image processing and statistical analysis of fMRI Data.

Jun Long received the B.S., M.S., and Ph.D. degrees from Central South University, Hunan, China, in 1996, 2004, and 2011, respectively.

He is currently a Professor and Vice Dean at the School of Information Science and Engineering, Central South University, Changsha, China. His current research interests include biomedical engineering, big data mining, and knowledge management.

Zhishun Wang (M'99–SM'99) received the Ph.D. degree in signal processing from Southeast University in 1997 and the doctoral thesis was granted "Excellent Doctoral Thesis Award in Year 2000" by the Academic Committee of the State Council of China. He is a Senior Member in signal processing society. He has published more than 140 journal and conference papers and received a number of Young Investigator Awards in biomedical signal processing field.

He is currently an Associate Professor in Brain Imaging with the Department of Psychiatry at Columbia University, New York, NY, USA, and New York State Psychiatric Institute, New York, where he is leading a group to conduct pioneered research to discover brain circuits that govern human cognitive process and psychiatric disorders. He has been extensively working on brain imaging and its application to the research of human cognitive process and childhood psychiatry with an emphasis on signal processing of functional magnetic resonance imaging and its integration with other modalities of brain imaging techniques. His research interests include functional and structural MRI, multidimensional signal/image processing, neural networks, machine learning, chaos and fractal in the brain and the gut, independent component analysis, wavelet, functional and effective brain connectivity.